J. Fluid Mech. (2022), *vol*. 946, A7, doi:10.1017/jfm.2022.567

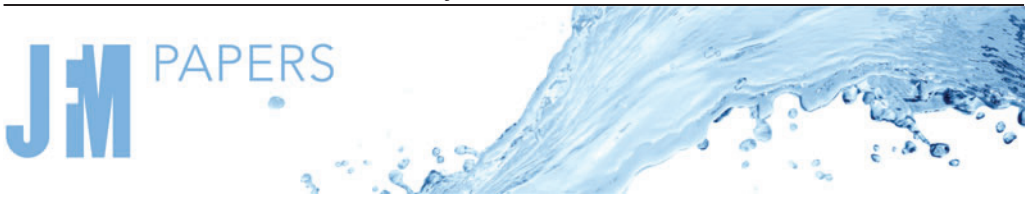

Eccentricity effect on horizontal capillary emptying

Dongwen Tan[1], Xinping Zhou[1,2,†], Gang Zhang[1,3], Chengwei Zhu[1,3] and Chenyu Fu[1]

[1]School of Mechanical Science and Engineering, Huazhong University of Science and Technology, Wuhan 430074, PR China

[2]State Key Laboratory of Digital Manufacturing Equipment and Technology, Huazhong University of Science and Technology, Wuhan 430074, PR China

[3]Department of Mechanics, Huazhong University of Science and Technology, Wuhan 430074, PR China

(Received 13 January 2022; revised 6 June 2022; accepted 27 June 2022)

This paper theoretically studies the effect of eccentricity on the conditions of capillary emptying (determined by critical Bond number) in a horizontal annular tube in a downward gravity field. Experiments are conducted to compare with theoretical results. We find that non-horizontal eccentricity can lead to the occurrence of a re-entrant liquid-state transition (from liquid non-occlusion to liquid plug to liquid non-occlusion) with increasing Bond number, when the eccentricity (e) or inner-to-outer radius ratio (χ) is large enough, and the two liquid non-occlusion states correspond to different emptying mechanisms dominated by the gravity effect and the 'wedge' effect, respectively. Existence of the re-entrant transition is accompanied by occurrence of unconditional liquid non-occlusion at large enough or small enough contact angles regardless of Bond numbers. The critical Bond numbers at a contact angle γ for vertical upward eccentricity are equal to those at a contact angle $180^\circ - \gamma$ for vertical downward eccentricity. In a parameter space (γ, $e/(1-\chi)$), the region with the re-entrant transition becomes larger with the eccentric angle varying from 0° (horizontal) to 90° (vertical). Optimization of geometrical parameters and inner and outer contact angles can lead to better effect of capillary emptying. This paper provides a very effective scheme for removing a liquid blockage from a capillary in optofluidics/microfluidics.

Key words: capillary flows

† Email address for correspondence: xpzhou08@hust.edu.cn

1. Introduction

Some small multiphase fluid containers may be blocked by liquid or gas. Fluid plugs occur in many processes, and may shut down the oxidizer flow in fuel cells (Zhang, Yang & Wang 2006), cause gas embolization in cardiovascular vessels (Lee, Wu & Li 2020), or degrade the transporting efficiency of the liquid propellant in fuel tanks of spacecraft under microgravity (Chen & Collicott 2006). It is of great importance to remove such fluid plugs by capillary emptying, which is capillary non-occluding and does not mean the tube would completely empty here.

Generally, the multiphase fluid interface deformation in a capillary can be affected considerably by a transverse body force (if the force exists). The critical Bond number is used as the critical parameter of determining the existence or non-existence of capillary plugs in a horizontal tube in a gravity field. The Bond number is given by

$$Bo = \delta^2/l_{ca}^2, \tag{1.1}$$

where δ is the characteristic length of the capillary tube with a cross-section of arbitrary geometry and $l_{ca} = \sqrt{\sigma/\rho g}$ is the capillary length, with surface tension σ between liquid and gas, (positive) density difference ρ between liquid and gas and gravitational acceleration g. Generally, in a horizontal open or concentric annular capillary in a downward gravity field (Manning, Collicott & Finn 2011; Manning & Collicott 2015; Rascón, Parry & Aarts 2016; Zhu, Zhou & Zhang 2020; Zhou *et al.* 2021), the criterion for the non-existence of capillary plugs is

$$Bo > Bo_c, \tag{1.2}$$

where Bo_c is the critical Bond number. In this case, the emptying of a capillary tube is dominated by the gravity effect. The characteristic lengths of capillaries corresponding to the critical Bond numbers during investigation of the problem are mainly of millimetre or micrometre (see Parry *et al.* 2012) sizes. From the theory in a transverse body force field (Manning *et al.* 2011; Manning & Collicott 2015; Rascón *et al.* 2016; Zhu *et al.* 2020; Zhou *et al.* 2021) developed from the theory in microgravity (Concus & Finn 1969; Finn 1986), the critical Bond number can be obtained at a given contact angle.

New shapes of tubes for liquid non-occlusion in a transverse body force field have been investigated theoretically. A flattened ice-cream cone cylinder was designed by Manning *et al.* (2011) for liquid non-occlusion. The critical Bond number for a rectangular tube was found to decrease when using a large enough width-to-height ratio of cross-section (Manning & Collicott 2015) and to further decrease when reducing the bottom contact angle and a side contact angle and increasing the top contact angle and the other side contact angle (Zhu *et al.* 2020). The critical Bond number was able to be changed by using other shapes (ellipse and triangle) and different orientations (Rascón *et al.* 2016). For an existing small tube facing the problem of liquid plugs, how to remove the existing liquid plugs is of great importance. However, replacing a liquid-plugged tube by a new tube of a different shape having larger emptying capacity is a difficult process. Instead, a simple possible measure should be sought. In this situation, the idea of using an eccentrically positioned rod to avoid liquid plugs in zero gravity was proposed by Smedley (1990) and Pour & Thiessen (2019); Zhou *et al.* (2021) found that the insertion of a rod at the centre of a horizontal liquid-plugged tube in a downward gravity field may help to remove liquid plugs from the tube.

Little experimental work about fluid occlusion and emptying in a capillary tube has been conducted to date. Verma *et al.* (2020) conducted experimental research on the generalized

emptying criteria for finite-length capillaries by taking the contact line pinning at the sharp edge into consideration, and their experiment properly validates the theoretical conclusion that a different bottom contact angle from the top contact angle can cause the critical Bond number to vary (Parry *et al*. 2012; Zhu *et al*. 2020). Zhou *et al.* (2021) performed an experimental study to validate their theoretical finding that the insertion of a rod into a tube at its centre helps to remove liquid occlusion.

Special tube structure with a rod inserted into the tube at an eccentric position has applications in other fluidic systems (Smedley 1990; Carrasco-Teja *et al.* 2008; Nikitin, Wang & Chernyshenko 2009; Choueiri & Tavoularis 2015; Pour & Thiessen 2019; Renteria & Frigaard 2020; Lamarche-Gagnon & Tavoularis 2021). It is worth noting that fluid occlusion (in a liquid–gas system) even at zero Bond number can be prevented by the use of eccentricity of annular tube cross-section (Smedley 1990; Pour & Thiessen 2019) due to the 'wedge' effect, i.e. the effect of wedge-shaped regions (Concus & Finn 1969; Protiere, Duprat & Stone 2013; Reyssat 2015; Rascón *et al.* 2016). Can the 'wedge' effect (produced by the eccentricity) together with the gravity effect help to remove (avoid) fluid occlusion from (in) a horizontal annular tube in a downward gravity field for a larger range of contact angles? How do different eccentric angles influence fluid non-occlusion? Is the conventional criterion (1.2) for the non-existence of capillary plugs still applicable? Answers to these interesting questions have not been reported to date.

In this paper, we take a horizontal tube structure with a rod inserted eccentrically into a circular tube as an example to answer the above questions. We extend the research of Zhou *et al.* (2021) to the effect of eccentricity on the emptying conditions of a horizontal annular capillary, observe new phenomena that have not been reported in a horizontal open (Manning *et al.* 2011; Manning & Collicott 2015; Rascón *et al.* 2016; Zhu *et al.* 2020) or concentric annular tube (Zhou *et al.* 2021) or in an eccentric annular tube in zero gravity (Smedley 1990; Pour & Thiessen 2019) and find greater emptying capacity than in Zhou *et al.* (2021) to a large extent. In § 2, the mathematical model for a tube with a general cross-section of irregular geometry (e.g. an eccentric annulus) is developed. In § 3, the eccentricity effect on the critical Bond numbers and the emptying mechanisms is theoretically investigated by changing the magnitude and direction of eccentricity, the inner-to-outer radius ratio and the contact angles on the inner rod wall and the outer tube wall, and the effect of non-equal inner and outer contact angles is also examined. In § 4, an experiment is done for validation of the mathematical model. In § 5, main conclusions are drawn.

2. Mathematical model

Figure 1 shows a schematic of a gas–liquid interface in a general cross-section of an infinitely long horizontal circular tube with a horizontal rod inserted into it at an eccentric position in a downward gravity field in Cartesian coordinates (x, y, z). In this paper, for the irregular geometry of tube cross-section, the outer tube centre O lies on the x axis, while the centroid of the annulus is not necessarily on the x axis. The radius ratio of the tube χ is defined as the ratio of the rod radius R_i to the radius of the outer tube R_o. The displacement d is non-dimensionalized by the characteristic length R_o to obtain the eccentricity as $e = d/R_o$. The Bond number of the eccentric annular tube is given by $Bo = (R_o/l_{ca})^2$. The annular gap between the tube and the inside rod is filled with liquid and gas two-phase immiscible fluids, both of which have very large fixed volumes.

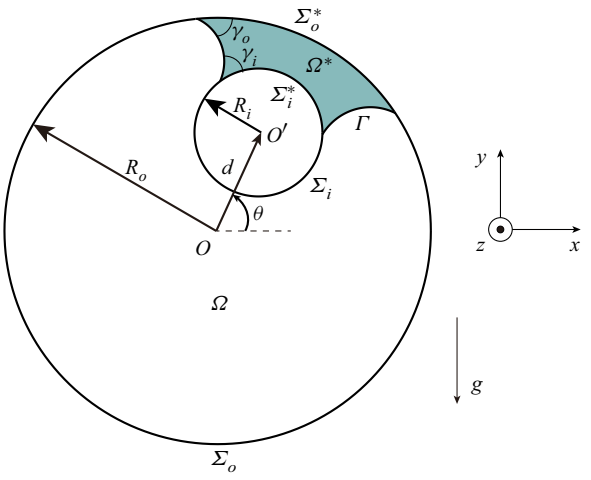

Figure 1. Schematic of general cross-section of liquid partially filling a horizontal circular tube of radius R_o with a rod of radius R_i inserted into it at an eccentric position in a downward gravity field. The displacement d is defined as the distance of the rod centre O' away from the outer tube centre O. The eccentric angle θ is measured counterclockwise, starting from the positive x axis. The gas–liquid interface Γ meets the inner and outer walls at contact points with inner and outer contact angles γ_i and γ_o. The annular gap has total area Ω and total inner and outer perimeters Σ_i and Σ_o, while the liquid has area Ω^* and wetting inner and outer perimeters Σ_i^* and Σ_o^*.

The three-dimensional (3-D) Young–Laplace equation due to gravity and the surface tension force can be expressed as (Finn 1986)

$$\nabla \cdot \boldsymbol{T}u = l_{ca}^{-2} y + \lambda, \quad \boldsymbol{T}u = \frac{\nabla u}{(1 + |\nabla u|^2)^{0.5}}, \tag{2.1a,b}$$

where $u(x, y)$ describes the shape of the 3-D liquid surface and λ is a Lagrange parameter. The following boundary conditions are satisfied:

$$\boldsymbol{v_i} \cdot \boldsymbol{T}u = \cos\gamma_i, \quad \text{on the inner rod wall,} \tag{2.2a}$$

$$\boldsymbol{v_o} \cdot \boldsymbol{T}u = \cos\gamma_o, \quad \text{on the outer tube wall,} \tag{2.2b}$$

where $\boldsymbol{v_i}$ is the unit exterior normal to the tube on the inner perimeter Σ_i of the annular cross-section, $\boldsymbol{v_o}$ is the unit exterior normal to the tube on the outer perimeter Σ_o and γ_i and γ_o are the inner and outer contact angles, respectively. According to the Green formula, the following term can be given based on (2.2*a*) and (2.2*b*):

$$\int_\Omega \operatorname{div} \boldsymbol{T}u = \int_{\Sigma_i} \boldsymbol{v} \cdot \boldsymbol{T}u + \int_{\Sigma_o} \boldsymbol{v} \cdot \boldsymbol{T}u = |\Sigma_i| \cos\gamma_i + |\Sigma_o| \cos\gamma_o. \tag{2.3}$$

The Lagrange multiplier λ is determined by the liquid volume and container, but is not related to the liquid volume for a capillary of a constant cross-section. By integration of (2.1*a*) and employing (2.3), one obtains

$$\lambda = \frac{1}{|\Omega|}\left(\int_\Omega \operatorname{div} \boldsymbol{T}u - l_{ca}^{-2}\Upsilon\right) = \frac{1}{|\Omega|}(|\Sigma_i| \cos\gamma_i + |\Sigma_o| \cos\gamma_o - l_{ca}^{-2}\Upsilon), \quad \Upsilon = \int_\Omega y. \tag{2.4}$$

For a circular tube with a rod inserted at an eccentric position, λ is rewritten as

$$\lambda = \frac{2(R_o \cos\gamma_o + R_i \cos\gamma_i) + l_{ca}^{-2} R_o R_i^2 e \sin\theta}{R_o^2 - R_i^2} = \frac{2(\cos\gamma_o + \chi \cos\gamma_i) + l_{ca}^{-2} R_o^2 \chi^2 e \sin\theta}{R_o(1-\chi^2)}, \tag{2.5}$$

where θ is the eccentric angle. For the concentricity case and the horizontal eccentricity case, the centroid of the annulus just lies on the x axis, and λ is reduced to (Zhou *et al.* 2021)

$$\Upsilon = \int_{\Omega} y = 0, \quad \lambda = \frac{|\Sigma_i| \cos\gamma_i + |\Sigma_o| \cos\gamma_o}{|\Omega|} = \frac{2(\cos\gamma_o + \chi\cos\gamma_i)}{R_o(1-\chi^2)}. \tag{2.6a,b}$$

If $\gamma_i = \gamma_o = 90^\circ$, then (2.5) is reduced to

$$\lambda = \frac{l_{ca}^{-2} R_o \chi^2 e \sin\theta}{1-\chi^2}. \tag{2.7}$$

Under the critical condition of transition between liquid plug and liquid non-occlusion (corresponding to the critical Bond number), the tongue of a large 3-D droplet can be seen to be infinitely long with its cross-section being translationally invariant. The total free energy of a 3-D droplet that contains the free surface energy, the wetting energy, the gravitational energy and a liquid internal energy term imposing a volumetric constraint on the problem is finite. Thus, the total free energy per unit length of the tongue corresponding to the critical Bond number should be equal to zero. On this occasion, the 3-D problem of determining the critical conditions of transition between liquid plug and liquid non-occlusion is reduced to an associated two-dimensional (2-D) problem. The functional denoting the total free energy of a drop per unit length of liquid tongue based on a general cross-section of an annular capillary is given by (Zhou *et al.* 2021)

$$\Phi = |\Gamma| - (|\Sigma_o^*| \cos\gamma_o + |\Sigma_i^*| \cos\gamma_i) + l_{ca}^{-2} \int_{\Omega^*} y \,\mathrm{d}x\,\mathrm{d}y + \lambda |\Omega^*|, \tag{2.8}$$

where Γ is the arc length of the gas–liquid interface and the gas–liquid interface can be determined by the Young–Laplace equation in two dimensions (Bhatnagar & Finn 2016; Zhou & Zhang 2017):

$$\frac{\mathrm{d}}{\mathrm{d}x} \frac{y_x}{\sqrt{1+y_x^2}} = l_{ca}^{-2} y + \lambda, \tag{2.9}$$

where $y_x = \mathrm{d}y/\mathrm{d}x$, with the inner and outer contact angle conditions satisfied, Ω^* is the liquid interior area and Σ_i^* and Σ_o^* are the wetting inner and outer perimeters, respectively (see figure 1). The critical Bond number can be determined by solving the following equation (Finn 1986; Manning *et al.* 2011; Rascón *et al.* 2016; Zhou *et al.* 2021):

$$\Phi = 0. \tag{2.10}$$

Table 1 gives the computational procedure for obtaining the critical Bond number(s) of an eccentric annular capillary with a given geometry for a set of inner and outer contact angles when the critical Bond number(s) exists. The total free energy of the droplet in a tube always reaches the minimum possible value and, accordingly, at the fourth step of the computational procedure in table 1, the interface with the minimum energy Φ_{min} is chosen among all the possible interfaces calculated from (2.9) satisfying the contact angle conditions at a given Bond number. The non-existence of a liquid plug for a Bond

1. Treat *Bo* as the independent variable.
2. Find all the possible gas–liquid interfaces calculated from (2.9) satisfying the contact angle conditions by gradually changing the contact points along the entire perimeters Σ_i and Σ_o.
3. Calculate the values of the energy functional corresponding to the possible interfaces by (2.8).
4. Find and choose the interface with the minimum energy Φ_{min} among the possible interfaces.
5. Vary *Bo* from 0 to a large enough value to find the critical Bond number(s) at which (2.10) is satisfied.

Table 1. Computational procedure to obtain the critical Bond number(s) for a given capillary tube geometry and specified contact angles when the critical Bond number(s) exists.

number can be determined by judging the sign (positive or negative) of the value of the minimum energy Φ_{min}. The case of $\Phi_{min} < 0$ for a Bond number indicates non-existence of a liquid plug, while $\Phi_{min} > 0$ for a Bond number permits an occluding liquid surface in the capillary tube (Manning *et al.* 2011).

For $\gamma_o = \gamma_i = 90^\circ$, the Lagrange multiplier λ and the critical Bond number for the horizontal eccentricity case are analytically obtained as

$$\lambda = 0, \quad Bo_c = \frac{3}{(\chi + 0.5)^2 + 0.75}, \tag{2.11a,b}$$

which are the same as those for the concentricity case (Zhou *et al.* 2021).

3. Results and discussion

The inside rod may be located at arbitrary eccentric positions in various directions in a tube. For vertical upward and downward eccentricities, the gas–liquid interface is symmetric with respect to the vertical axis of symmetry but the centroid of the annulus has a vertical displacement from the centre of the outer tube O. While, for horizontal eccentricity, the centroid of the annulus is kept at the same height as the outer tube centre, but the interface is not symmetric with respect to the vertical axis of symmetry. For eccentricity in directions other than vertical and horizontal directions, the interface is not symmetric with respect to the vertical axis of symmetry and the centroid of the annulus deviates slantly from the outer tube centre. These lead to the complexity of computation and analysis regarding this problem. The vertical and horizontal eccentricities are considered as the basic forms of eccentricity in terms of studying the eccentricity effect. In the following sections, we initially analyse the cases of vertical and horizontal eccentricities and then analyse the cases of inclined eccentricity at different inclined angles under the conditions of equal inner and outer contact angles. The contact angle studied here ranges from 1° to 179° at intervals of 1° and a local refinement around each kink is conducted. The effect of radius ratio is also discussed. The cases of non-equal inner and outer contact angles are finally investigated.

3.1. *Vertical eccentricity*

Consider an annular tube of vertical upward eccentricity. The eccentricity is restricted to be in a range $0 < e < 1 - \chi$, while the cases $e > 1 - \chi$ will be non-physical. The critical emptying lines (each being a plot of critical Bond number as a function of contact angle) of the annular tubes with three radius ratios $\chi = 0.1$, 0.4 and 0.7 and different vertical upward eccentricities for equal inner and outer contact angles ($\gamma_o = \gamma_i = \gamma$) are shown in figure 2. Due to the vertical eccentricity, the critical emptying line is not yet symmetric

about the vertical line $\gamma = 90°$. Interestingly, lower and upper critical emptying lines occur when the eccentricity or radius ratio is large enough. The two critical emptying lines start appearing at smaller eccentricity for larger radius ratio (for example, $e \geq 0.7$ for $\chi = 0.1$, $e \geq 0.3$ for $\chi = 0.4$ and $e \geq 0.05$ for $\chi = 0.7$), as shown in figure 2(*a–c*). Parameters Bo_{cl} and Bo_{cu} are defined as the critical Bond numbers on the lower and upper critical emptying lines, respectively. The lower and upper critical emptying lines touch the horizontal line $Bo = 0$ at a smaller contact angle $\gamma_{Bo_{cl}=0}$ (e.g. point *J* in figure 2*b*) and a larger contact angle $\gamma_{Bo_{cu}=0}$ (e.g. point *K* in figure 2*b*), respectively, and may intersect at the contact angle $\gamma_{Bo_{cl}=Bo_{cu}\neq 0}$ (e.g. point *I* in figure 2*b*).

Generally, there are two kinks of the critical emptying lines containing lower and upper lines for a not-so-large radius ratio (for example, $e = 0.8$ for $\chi = 0.1$ and $e = 0.4$ and 0.5 for $\chi = 0.4$), one of which is also the intersection point of the lower and upper critical emptying lines. Occurrence of the two kinks is attributed to the contact point jumps due to the transition among the three non-occluded liquid topologies represented by the cross-sections *D–F* in figure 2(*a*) or the cross-sections *C–E* in figure 2(*b*). However, there is one kink of the critical emptying lines containing lower and upper lines for a larger radius ratio (for example, only one kink existing at $e = 0.2$ or 0.25 for $\chi = 0.7$), and the kink is just the intersection point of the lower and upper critical emptying lines, as shown in figure 2(*c*). The reduction of the number of kinks by one as compared to the general case of a not-so-large radius ratio is attributed to the non-existence of the non-occluded liquid topology with the interface only meeting the outer wall due to the larger radius ratio. Additionally, for some smaller eccentricities (for example, $e = 0.7$ for $\chi = 0.1$, $e = 0.3$ for $\chi = 0.4$ and $e = 0.05$, 0.1 and 0.15 for $\chi = 0.7$), the two critical emptying lines do not interact, and this causes one kink to disappear.

The occurrence of lower and upper critical emptying lines is attributed to two solutions (two critical Bond numbers) of (2.10) obtained for each of the contact angles $\gamma_{Bo_{cl}=Bo_{cu}\neq 0} < \gamma \leq \gamma_{Bo_{cl}=0}$, corresponding to two critical Bond numbers (figure 3), which is different from only one solution (Bo_c) of (2.10) for the horizontal open (Manning *et al.* 2011; Manning & Collicott 2015; Rascón *et al.* 2016; Zhu *et al.* 2020) or concentric annular (Zhou *et al.* 2021) capillary in a normal downward gravity field. Besides the two critical Bond numbers for $\gamma_{Bo_{cl}=Bo_{cu}\neq 0} < \gamma \leq \gamma_{Bo_{cl}=0}$, there is only one Bo_c for $\gamma_{Bo_{cl}=0} < \gamma \leq \gamma_{Bo_{cu}=0}$ in the contact angle range of the critical emptying lines. For a contact angle ranging between $\gamma_{Bo_{cl}=Bo_{cu}\neq 0}$ and $\gamma_{Bo_{cl}=0}$, a re-entrant liquid state transition (i.e. transition from liquid non-occlusion to liquid plug and transition from liquid plug to liquid non-occlusion) with the Bond number increasing from 0 to a large enough value is found. In this case, the criterion (1.2) for the non-existence of capillary plugs is obviously not applicable. For the cases of two critical emptying lines, whether in the two-Bo_c contact angle range or in the one-Bo_c contact angle range, capillary plugs do not exist when the following condition is satisfied:

$$Bo < Bo_{cl} \quad \text{or} \quad Bo > Bo_{cu}. \tag{3.1}$$

As shown in figure 2, if $Bo < Bo_{cl}$, then liquid non-occlusion with the new topology where the liquid is trapped in the narrow region of the horizontal tube will occur due to the 'wedge' effect. Regarding the state of capillary plugs, the 3-D interfaces directly computed via Surface Evolver (Brakke 1992) for different Bond numbers between the lower and upper critical emptying lines at a representative contact angle of the tube ($\chi = 0.4$ and $e = 0.4$) are displayed in figure 2(*b*). When Bo is slightly above the lower critical emptying line, the upper tongue of the plugging liquid droplet is much longer than the lower tongue. When the lower critical Bond number is attained, the upper tongue can be seen to be

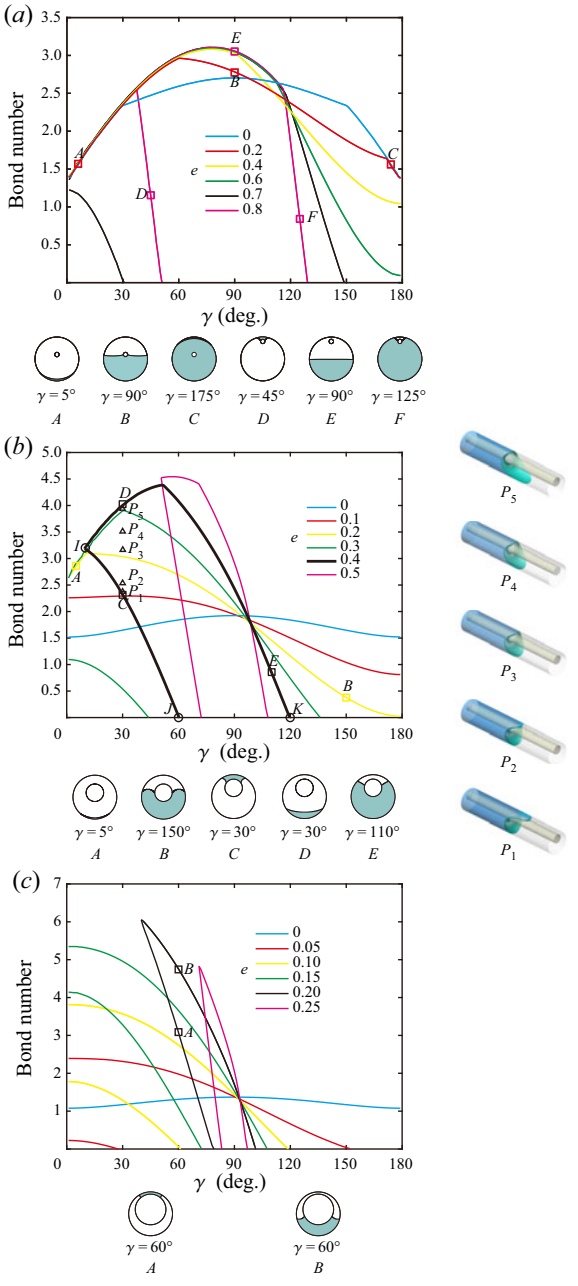

Figure 2. Critical Bond numbers of annular tubes with different vertical upward eccentricities for different radius ratios (*a*) $\chi = 0.1$, (*b*) $\chi = 0.4$ and (*c*) $\chi = 0.7$ versus contact angle $\gamma_o = \gamma_i = \gamma$. The squares denote the representative points each corresponding to a cross-section of the part of the interface that extends to infinite length at the critical Bond number. In (*b*), the circles on the black thick line denote three key points at $e = 0.4$. Points *I*, *J* and *K* correspond to the intersection point of the lower and upper critical emptying lines (i.e. the lines *IJ* and *IK*), $Bo_{cl} = 0$ and $Bo_{cu} = 0$, respectively. In the right-hand part of (*b*), 3-D interfaces (an oblique view) computed by Surface Evolver (Brakke 1992) at $\gamma = 30°$ for $e = 0.4$ for different Bond numbers correspond to the triangles denoting the points P_1, P_2, P_3, P_4 and P_5, respectively. For points P_1 and P_2, the upper tongue is longer than the lower tongue (the phenomenon for point P_2 does not seem apparent due to the oblique view, and accordingly a grey circle through the tip of the lower tongue denoting a cross-section of the outer tube is plotted to help understand the phenomenon for point P_2), while for points P_3, P_4 and P_5, the lower tongue is longer than the upper tongue.

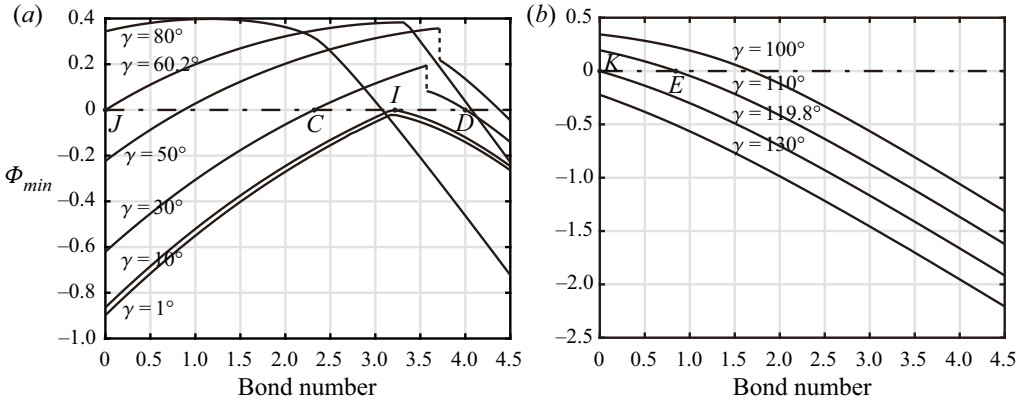

Figure 3. Minimum energy Φ_{min} (calculated at the fourth step of table 1) for an annular tube of vertical upward eccentricity ($\chi = 0.4$ and $e = 0.4$) for (*a*) the cases $\gamma_o = \gamma_i = \gamma < 90°$ and (*b*) the cases $\gamma_o = \gamma_i = \gamma > 90°$ versus Bond number. Points *C*–*E* and *I*–*K* correspond to *C*–*E* and *I*–*K*, respectively, as presented in figure 2(*b*). The dot-dashed line denotes the straight line for $\Phi_{min} = 0$. In (*a*), each dashed line (a discontinuous segment of the line of Φ_{min}) represents a jump due to the transition between different non-occluded liquid topologies corresponding to minimal total free energy.

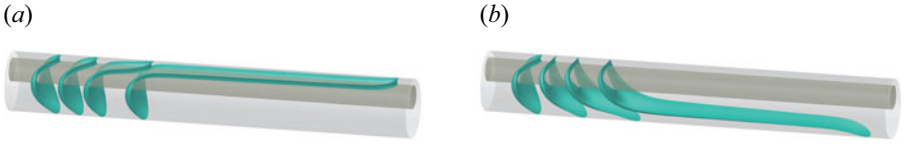

Figure 4. Schematic of evolution of the 3-D interface (an oblique view) (*a*) as the Bond number gradually decreases (from left to right) and approaches the lower critical Bond number and (*b*) as the Bond number gradually increases (from left to right) and approaches the upper critical Bond number. Some representative 3-D interfaces computed using Surface Evolver (Brakke 1992) are integrated in a horizontal eccentric annular tube.

infinitely long. Crossing the lower critical emptying line by decreasing *Bo* can lead to the transition from liquid plug to liquid non-occlusion. With *Bo* increasing, the lower tongue of the plugging liquid droplet gradually becomes longer, which is accompanied by shortening of the upper tongue. When *Bo* approaches the upper critical emptying line, the lower tongue is much longer than the upper tongue (figure 4). When the upper critical Bond number is attained, the lower tongue also can be seen to be infinitely long. Crossing the upper emptying line by increasing *Bo* can induce the transition from liquid plug to liquid non-occlusion. The co-occurrence of upper tongue receding and lower tongue advancing is attributed to the gradual increase of the gravity effect relative to the 'wedge' effect with the increase of *Bo*. As expected, if $Bo > Bo_{cu}$, then liquid non-occlusion with the topology where the liquid is wrapped in the wide region will occur due to the larger gravity leading to disappearance of the 'wedge' effect in this case.

The contact angles of the lower critical emptying line are smaller than 90°. For the contact angle range $\gamma_{Bo_{cl}=Bo_{cu}\neq 0} < \gamma < \gamma_{Bo_{cl}=0}$, a sufficiently small capillary has a sufficiently small Bond number smaller than Bo_{cl} except at the contact angles adjacent to the contact angle $\gamma_{Bo_{cl}=0}$ (e.g. point *J* in figure 2*b*), and in this case, the sufficiently small capillary can be of approximate liquid non-occlusion. If $\gamma > \gamma_{Bo_{cu}=0}$ or $< \gamma_{Bo_{cl}=Bo_{cu}\neq 0}$, the capillary tube will be in a state of unconditional liquid non-occlusion, no matter what the size of the capillary tube cross-section. Generally, a sufficiently small horizontal

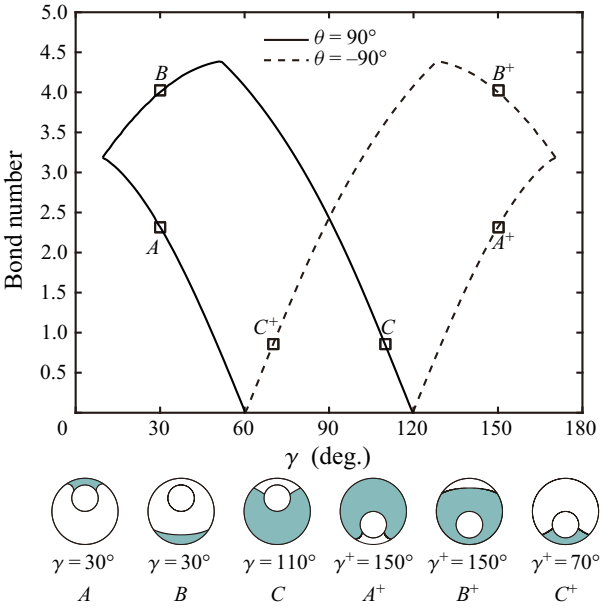

Figure 5. Critical Bond numbers of annular tubes with vertical upward ($\theta = 90°$) and downward ($\theta = -90°$) eccentricities $e = 0.4$ for representative radius ratio $\chi = 0.4$ versus contact angle $\gamma_o = \gamma_i = \gamma$.

capillary tube in a downward gravity field will be approximately or unconditionally liquid non-occluding for the contact angle range excluding $\gamma_{Bo_{cl}=0} \leq \gamma \leq \gamma_{Bo_{cu}=0}$. The total contact angle range $\Delta\gamma$ of approximate and unconditional liquid non-occlusions is defined as

$$\Delta\gamma = \gamma_{Bo_{cl}=0} + 180^\circ - \gamma_{Bo_{cu}=0}. \tag{3.2}$$

According to the results calculated using the model, the two contact angles of zero critical Bond number have the following relationship:

$$\gamma_{Bo_{cl}=0} = 180^\circ - \gamma_{Bo_{cu}=0}. \tag{3.3}$$

This relationship (3.3) also can be obtained from Appendix A. Substituting (3.3) into (3.2), $\Delta\gamma$ is rewritten as $\Delta\gamma = 2\gamma_{Bo_{cl}=0}$. It is also found from figure 2 that the value of $\Delta\gamma$ can be increased by an increase of vertical eccentricity or radius ratio.

Here, we discuss the relationship between the critical Bond numbers for vertical downward eccentricity and those for vertical upward eccentricity. Under the condition of equal magnitude of eccentricity, the perimeter of the tube cross-section for vertical downward eccentricity and that for vertical upward eccentricity are symmetric with respect to the horizontal axis. In this case, from Appendix A, a gas–liquid interface for vertical downward eccentricity at a contact angle $\gamma^+ = 180^\circ - \gamma$ that is symmetric to a given interface for vertical upward eccentricity at a contact angle γ with respect to the horizontal axis can be found, and the critical Bond number(s) for the vertical downward eccentricity at contact angle $\gamma^+ = 180^\circ - \gamma$ is equal to that for the vertical upward eccentricity at contact angle γ, as shown in figure 5. Accordingly, an eccentric angle range from 0° to 90° is sufficient when studying the effect of eccentric angle in the following sections.

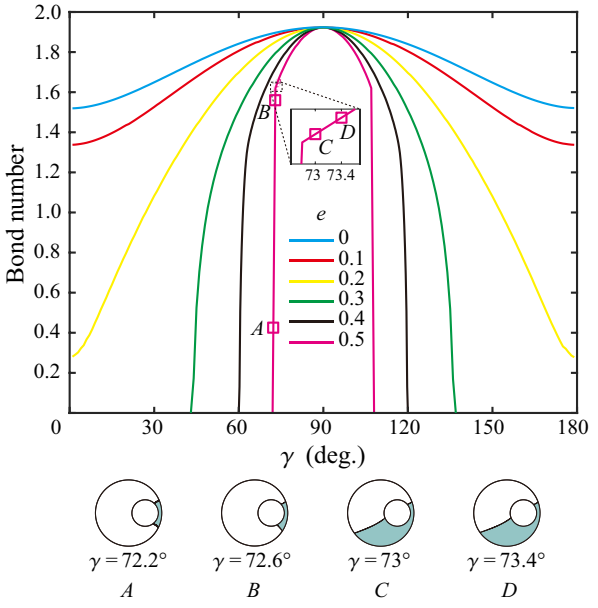

Figure 6. Critical Bond numbers of annular tubes with different horizontal eccentricities for representative radius ratio $\chi = 0.4$ versus contact angle $\gamma_o = \gamma_i = \gamma$. An enlarged view of the line segments around the left kink of the curve for $e = 0.5$ is shown. Contact angle refinement for $e = 0.4$ is conducted in order to avoid the appearance of false kinks.

3.2. *Horizontal eccentricity*

Consider an annular tube of horizontal eccentricity. The critical emptying lines of annular tubes with different horizontal eccentricities and representative radius ratio $\chi = 0.4$ for $\gamma_o = \gamma_i = \gamma$ are shown in figure 6. The critical emptying line is symmetric about the vertical line $\gamma = 90°$, which can be obtained from Appendix A. With the eccentricity increasing, the critical emptying line gradually drops. However, the maximums for different horizontal eccentricities reached at $\gamma = 90°$ are equal for a certain radius ratio and are reduced with the radius ratio increasing. These can be directly derived from (2.11*b*). Furthermore, the case of two critical emptying lines does not yet occur. This is attributed to the geometric feature that the centroid of the eccentric annulus lies on the x axis, which is the same as the case of a concentric annulus. As shown in the figure, the critical Bond number reaches zero at a contact angle for $e \geq 0.3$, and the contact angle range for unconditional liquid non-occlusion regardless of Bond numbers increases with the horizontal eccentricity increasing. Note that a kink appears at $\gamma \approx 72.8°$ for the case $e = 0.5$ due to the occurrence of contact point jump (see configurations B and C in figure 6).

3.3. *Inclined eccentricity*

After the discussion about the vertical and horizontal eccentricity effects, we want to know what the vertical–horizontal mixed eccentricity effect (i.e. the inclined eccentricity effect) is on the critical Bond number. We take an eccentric angle $\theta = 45°$ as an example to analyse the cases of inclined eccentricity (see figure 7*a*). As expected, $\Delta\gamma$ increases with inclined eccentricity (at a fixed eccentric angle) or radius ratio increasing. Interestingly, $\Delta\gamma$ remains constant with θ changing from 0° to 90° at intervals of 22.5° (see figure 7*b*). This is attributed to the fact that the two contact angles $\gamma_{Bo_{cl}=0}$ and $\gamma_{Bo_{cu}=0}$ determining

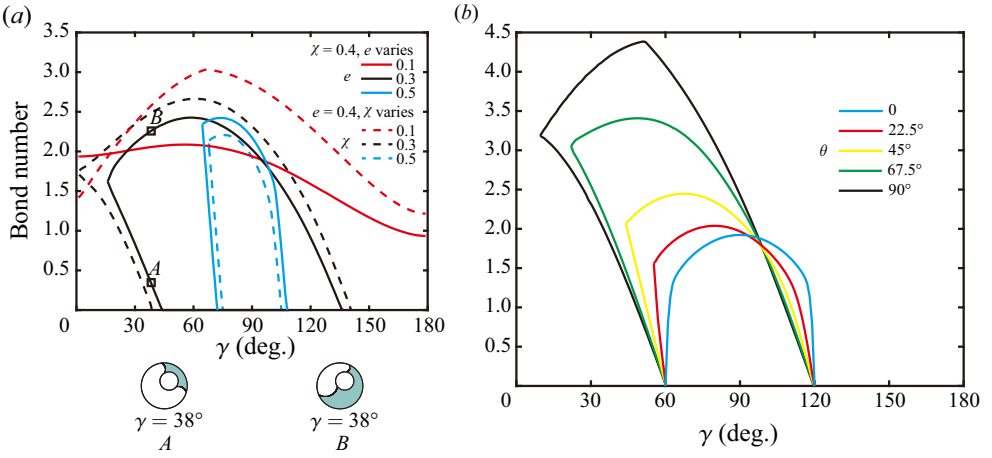

Figure 7. Critical Bond numbers of annular tubes with (*a*) different radius ratios and different eccentricities for eccentric angle $\theta = 45°$ and with (*b*) radius ratio $\chi = 0.4$ and eccentricity $e = 0.4$ for different eccentric angles versus contact angle $\gamma_o = \gamma_i = \gamma$.

the value of $\Delta\gamma$ are obtained in zero gravity, in which all the cases are not related to the eccentric angle.

3.4. *Phase diagram*

From the above analysis, it is found that the states are affected by the magnitude and direction of eccentricity, the radius ratio and the contact angles. In order to demonstrate this problem more clearly, the boundaries among four states, i.e. non-physical state, unconditional liquid non-occlusion, one Bo_c at a contact angle (gravity-dominated emptying mechanism) and two Bo_c at a contact angle (gravity and 'wedge' emptying mechanisms), in a space (γ, $e/(1-\chi)$) for $\gamma_o = \gamma_i = \gamma$ are plotted in figure 8. In this figure, the horizontal dashed line, above which is non-physical, is determined by $e/(1-\chi) = 1$, and the curves going though points J and K correspond to zero critical Bond number. The solutions (γ, $e/(1-\chi)$) for (2.10) at zero Bond number also can be determined theoretically based on the geometrical relationship (Pour & Thiessen, 2019), which is discussed in Appendix B.

The cases as shown in figure 8 are the cases of $\gamma_i = \gamma_o$. As shown in figure 8(*a*), in the parameter space (γ, $e/(1-\chi)$), the two boundary lines of the one-Bo_c region (i.e. the lines corresponding to zero critical Bond number) can be theoretically determined using the above solving method. The two-Bo_c cases and unconditional liquid non-occlusion cases may occur for $e/(1-\chi)$ ranging between 0.3376 and 1, and they would not exist for $e/(1-\chi) < 0.3376$ representing small enough eccentricity and small enough radius ratio. The two boundary lines of the one-Bo_c region do not change with the direction of eccentricity. In contrast, the boundary line between the left unconditional liquid non-occlusion region and the two-Bo_c region cannot be described theoretically and gradually drops (the two-Bo_c region in the parameter space becomes smaller) with θ decreasing from 90° to 0°, and it coincides with the left boundary line of the one-Bo_c region when $\theta = 0°$. This again illuminates that the two-Bo_c cases would not arise for horizontal eccentricity, as discussed in § 3.2. The two-Bo_c cases only occur at $\gamma < 90°$ and the range of $e/(1-\chi)$ corresponding to the cases becomes larger with γ decreasing.

As shown in figure 8(*b*), with the radius ratio increasing, the two-Bo_c region is enlarged, and the two boundary lines of the one-Bo_c region clearly drop, but the maximum value

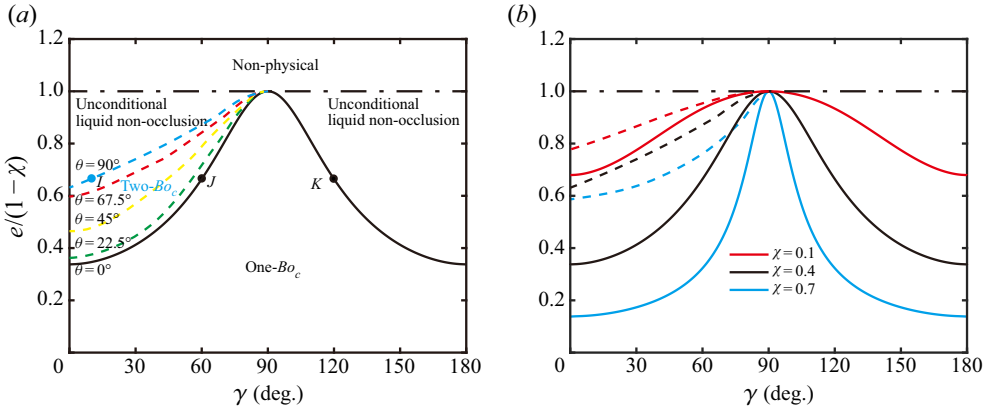

Figure 8. (*a*) Phase diagram in a space (γ, $e/(1-\chi)$) for different eccentric angles for $\chi = 0.4$ and (*b*) boundary lines in the parameter space for vertical eccentricity $\theta = 90°$ and different radius ratios $\chi = 0.1$, 0.4 and 0.7. Equal inner and outer contact angles are used: $\gamma_o = \gamma_i = \gamma$. In (*a*), boundaries among four states are presented for different eccentric angles. With the eccentric angle varies, the boundary line (dashed line) between the left unconditional liquid non-occlusion region and the two-Bo_c region changes, while the two boundary lines (solid lines) corresponding to zero critical Bond number do not change. Points *I*–*K* correspond to *I*–*K*, respectively, as presented in figure 2(*b*). The blue text annotation corresponds to the region between the blue dashed line and the solid line through point *J*, representing the two-Bo_c region in the parameter space for the case of vertical eccentricity $\theta = 90°$. In (*b*), the dashed line corresponds to the case denoted by the solid line in the same colour.

is kept constant at $\gamma = 90°$. The value of $\Delta\gamma$ also increases largely. This implies that increasing the radius ratio can effectively enhance the possibility of liquid non-occlusion in a small enough eccentric annular capillary.

3.5. *Non-equal inner and outer contact angles*

The above analysis is based on $\gamma_o = \gamma_i$. The effect of $\gamma_o \neq \gamma_i$ is examined in this section. The variation of the parameter $e/(1-\chi)$ with γ_o, and the variation of $\Delta\gamma_o$ (defined as the outer contact angle range of approximate and unconditional liquid non-occlusions at a fixed value of γ_i) with $e/(1-\chi)$ for different inner contact angles are compared with those for $\gamma_o = \gamma_i$ (see figure 9). According to Appendix A, under zero gravity, for an eccentric annular tube, if the minimal energy ϕ_{min} at contact angles γ_o and γ_i is equal to 0, then $\Phi^{+}_{min} = 0$ will exist at contact angles $180° - \gamma_o$ and $180° - \gamma_i$. Accordingly, the boundary lines of the one-Bo_c region at contact angles γ_o and γ_i and those at contact angles $180° - \gamma_o$ and $180° - \gamma_i$ are symmetric with respect to the vertical line $\gamma_o = 90°$. The cases of $\gamma_i > 90°$ have not been included in this analysis.

The boundary lines of the one-Bo_c region for $\gamma_o \neq \gamma_i$ are not symmetric about the vertical line $\gamma_o = 90°$ except $\gamma_i = 90°$. With γ_i decreasing from 90° to 30°, the maximum gradually shifts to the right, which is accompanied by the reduction of the right unconditional liquid non-occlusion region, and the two-Bo_c region is enlarged (figure 9*a*). Moreover, the case $\gamma_o = \gamma_i$ is found to have the maximum value of $\Delta\gamma_o$ (figure 9*b*). Accordingly, the condition of $\gamma_o = \gamma_i$ is preferable in view of liquid non-occlusion in a small enough eccentric annular capillary.

4. Experimental validation

The mathematical model is developed to determine the critical emptying conditions for a tube with a cross-section of irregular geometry. By analysing the results calculated based

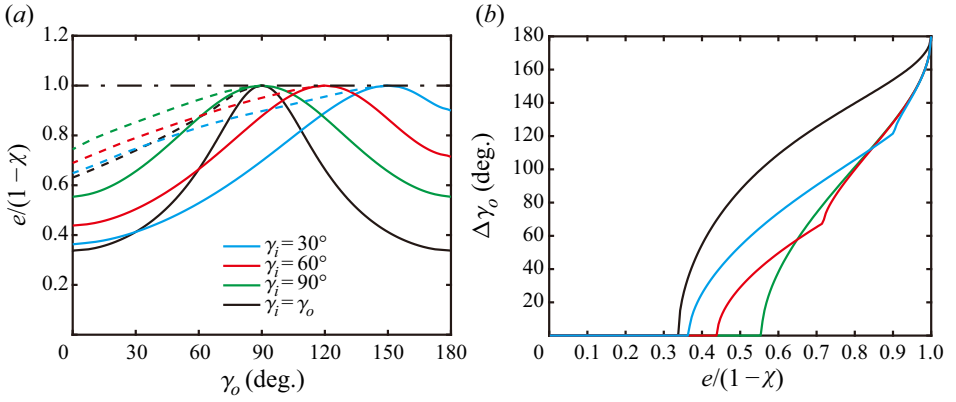

Figure 9. (*a*) Boundary lines in parameter space (γ_o, $e/(1-\chi)$) at $\chi = 0.4$ and $\theta = 90°$ for different inner contact angles versus outer contact angle γ_o and (*b*) outer contact angle ranges of approximate and unconditional liquid non-occlusions $\Delta\gamma_o$ for different inner contact angles versus $e/(1-\chi)$. In (*a*), the dashed line corresponds to the case denoted by the solid line in the same colour.

on the developed mathematical model, the vertical eccentricity has a notable effect on preventing capillary plugs in a tube, and a new phenomenology about the existence of the re-entrant liquid state transition is found. We take a vertical eccentricity as an example to conduct experiments to validate the new phenomenology found theoretically.

The silica glass capillary tubes used for the experiments had a length of 20 cm and were open at both ends, and the silica glass rods had a length of 30 cm. The contact angles of water on the glass surfaces used were measured using the sessile drop method to be approximately 30°. Long capillary tubes and rods were used in order to make the effect of contact line pinning at the sharp edge at both ends become negligible when studying the eccentricity effect here. The eccentric annular tube was formed by hanging the inside rod on two accessories manufactured using 3-D printing technology. The tubes and rods were cleaned using an ultrasonic cleaning machine before the experiments. Deionized water and air were used as the liquid and the gas, respectively. The fluids in capillaries exposed to two LED light sources were visualized by employing a Nikon D7200 camera mounted with Nikon Micro-NIKKOR 105 mm f/2.8G macro lenses.

The lower and upper critical emptying lines theoretically calculated using this model for an eccentric annular capillary of radius ratio $\chi = 0.5$ and vertical eccentricity $e = 0.27$ are displayed for experimental validation (see figure 10). The results of the experiments (radius ratio $\chi \approx 0.5$ and vertical eccentricity $e \approx 0.27$) for five different Bond numbers are obtained using capillaries of different sizes and rods of different sizes. We observe from the experiments that the vertically eccentric annular tube is not plugged by liquid for both the Bond number below the lower critical emptying line and the Bond number above the upper critical emptying line, while it is liquid-occluded for Bond number between the lower and upper critical emptying lines. It is concluded that the experiments well validate the existence of the re-entrant liquid state transition found theoretically. In a horizontal tube without eccentricity, due to the gravity effect, a liquid plug is generally accompanied by a morphology in which the lower tongue of the liquid droplet is longer than the upper tongue (see the lower photograph in figure 3*c* in Zhou *et al.* (2021)). In the experiments, when gravity is large enough (for example, the point denoted by a cross just above Q_2 in figure 10*a*), a liquid droplet morphology also exists with the lower tongue longer than the upper tongue similar to that in Zhou *et al.* (2021). Additionally, we found experimentally

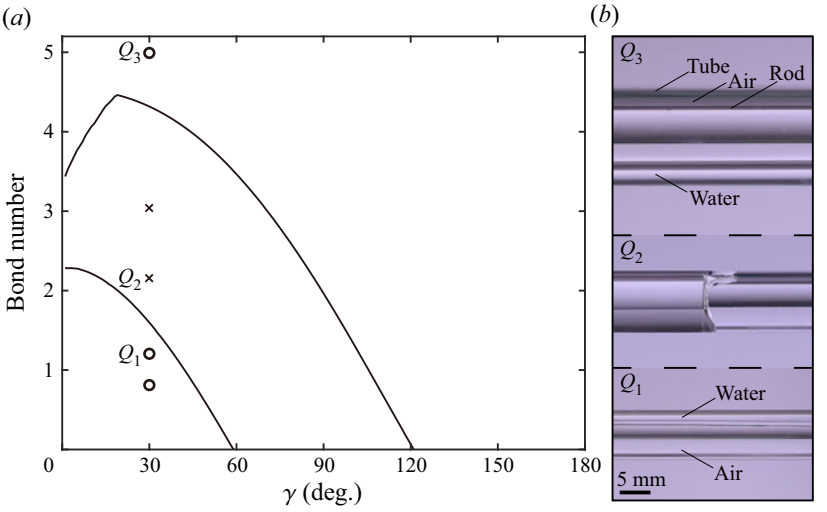

Figure 10. (*a*) Theoretical predictions for lower and upper 'critical emptying lines' ($Bo_c(\gamma)$, where $\gamma_o = \gamma_i = \gamma$) for a vertically eccentric annular capillary ($\chi = 0.5$ and $e = 0.27$) and experimental results. The circles (e.g. Q_1 and Q_3) indicate liquid non-occlusion and the crosses (e.g. Q_2) indicate that the liquid plug remains. For the three experimental cases Q_1, Q_2 and Q_3, different diameters of outer tubes at 5.95, 7.96 and 12.11 mm and the corresponding different sizes of rods are used, respectively, thus leading to different Bond numbers. Note that, as predicted by theory, a small tube (see Q_1) and a large tube (see Q_3) become non-occluding after rod insertion whereas a medium-sized tube remains blocked (see Q_2). (*b*) Photographs of the liquid occlusion or non-occlusion for the three experimental cases Q_1, Q_2 and Q_3 representing the liquid states related to the re-entrant transition with increasing *Bo*. Note that the contact angles at the lower section of the tube in the picture of Q_2 seem much larger than 30°. This is attributed to the 3-D liquid surface (meniscus) concave towards the gas and the position of the camera relative to the horizontal capillary.

that there is a case of liquid plugs where the upper tongue of the liquid droplet is a little longer than the lower tongue when *Bo* is a little above the lower critical emptying line (see Q_2 in figure 10*b*) because the 'wedge' effect gains an advantage over the gravity effect. This is in good agreement with the results directly computed via Surface Evolver (Brakke 1992) in 3-D mode.

5. Conclusions

The effect of eccentricity of an annular capillary with a rod inserted into a circular tube in a normal gravity field on the critical Bond number is investigated theoretically and experimentally. The effects of horizontal eccentricity, vertical eccentricity and inclined eccentricity are analysed. A phase diagram in a parameter space (γ, $e/(1-\chi)$) at different eccentric angles for $\gamma_o = \gamma_i$ is plotted. The influence of radius ratio and $\gamma_o \neq \gamma_i$ is examined. The following conclusions are drawn from the above analysis.

For the non-horizontal eccentricity case, the lower and upper critical emptying lines arise when the eccentricity or the radius ratio is large enough, and the lower critical emptying line for $\gamma_o = \gamma_i$ occurs at contact angles smaller than 90°. The critical Bond number(s) for the vertical upward eccentricity at a contact angle is equal to that for the vertical downward eccentricity at the supplementary contact angle. For the case of two critical Bond numbers at a contact angle, the re-entrant liquid state (liquid non-occlusion to plug to non-occlusion) transition occurs. For $Bo < Bo_{cl}$, the tube is non-occluding due to the 'wedge' effect. For $Bo_{cl} < Bo < Bo_{cu}$, the tube may be occluded by liquid and

receding of the upper tongue and advancing of the lower tongue occur together with an increase of Bo. When the lower (upper) critical Bond number is attained, the upper (lower) tongue can be seen to be infinitely long. For $Bo > Bo_{cu}$, the tube is also non-occluding due to larger gravity.

Existence of the two critical emptying lines is accompanied by the occurrence of unconditional liquid non-occlusion in a certain contact angle range ($\gamma > \gamma_{Bo_{cu}=0}$ and $<\gamma_{Bo_{cl}=Bo_{cu}\neq 0}$). A sufficiently small horizontal capillary tube will be approximately or unconditionally non-occluding if the contact angle is in the range $\Delta\gamma$ excluding those between the two contact angles at zero critical Bond number. In the parameter space (γ, $e/(1-\chi)$), with the eccentric angle increasing from 0° to 90°, the two-Bo_c region gradually becomes larger; however, the contact angle range $\Delta\gamma$ remains unchanged. The range $\Delta\gamma$ can be increased effectively by increasing the eccentricity and radius ratio. The case $\gamma_o = \gamma_i$ is found to have the maximum value of $\Delta\gamma_o$ compared with different cases of $\gamma_o \neq \gamma_i$. The condition $\gamma_o = \gamma_i$ is therefore preferable in view of liquid non-occlusion in a small enough eccentric annular capillary. This paper lays a solid foundation for more efficient use of inserting a rod into a horizontal capillary in terms of removing a liquid blockage, and for notably triggering the transition between a top flow path and a bottom flow path in optofluidic or microfluidic devices.

Funding. This research was supported in part by the National Natural Science Foundation of China (no. 11972170).

Declaration of interests. The authors report no conflict of interest.

Author ORCIDs.
Dongwen Tan https://orcid.org/0000-0002-2205-3045;
Xinping Zhou https://orcid.org/0000-0001-6340-5273;
Gang Zhang https://orcid.org/0000-0002-5236-4960;
Chenyu Fu https://orcid.org/0000-0001-6175-5421.

Appendix A

Under the critical emptying conditions, for a horizontal tube having a general cross-section Ω in an arbitrary geometrical shape (figure 11), the gas–liquid interface Γ: $y = y(x)$ is described by the 2-D Young–Laplace equation (2.9) with the boundary conditions $\boldsymbol{n_i} \cdot \boldsymbol{T}y = \cos\gamma_i$ and $\boldsymbol{n_o} \cdot \boldsymbol{T}y = \cos\gamma_o$. If the perimeters Σ_i^+ and Σ_o^+ of cross-section Ω^+ of a horizontal tube are respectively symmetric to Σ_i and Σ_o for the horizontal tube with respect to the horizontal axis (figure 11), $\gamma_i^+ = 180°-\gamma_i$ and $\gamma_o^+ = 180°-\gamma_o$, under the condition of other properties the same, a curve $\Gamma^+ : y^+ = -y(x)$ can be found, which satisfies the relationship

$$\frac{\mathrm{d}}{\mathrm{d}x}\frac{y_x^+}{\sqrt{1+(y_x^+)^2}} = l_{ca}^{-2}y^+ + \lambda^+, \tag{A1}$$

with the boundary conditions $\boldsymbol{n_i} \cdot \boldsymbol{T}y^+ = \cos\gamma_i^+$ and $\boldsymbol{n_o} \cdot \boldsymbol{T}y^+ = \cos\gamma_o^+$. According to the above features, the following relationship can be held by $\lambda^+ = -\lambda$, $|\Gamma| = |\Gamma^+|$, $|\Omega| = |\Omega^+|$, $|\Sigma_i| = |\Sigma_i^+|$, $|\Sigma_o| = |\Sigma_o^+|$, $|\Omega^*| = |\Omega^+| - |\Omega^{+*}|$, $|\Sigma_i^*| = |\Sigma_i^+| - |\Sigma_i^{+*}|$ and $|\Sigma_o^*| = |\Sigma_o^+| - |\Sigma_o^{+*}|$. In this case, the energy functional $\Phi = \Phi^+$. The critical Bond number(s) $Bo_c(\gamma_i, \gamma_o)$ for the tube with Ω is equal to $Bo_c(180° - \gamma_i, 180° - \gamma_o)$ for the tube with Ω^+.

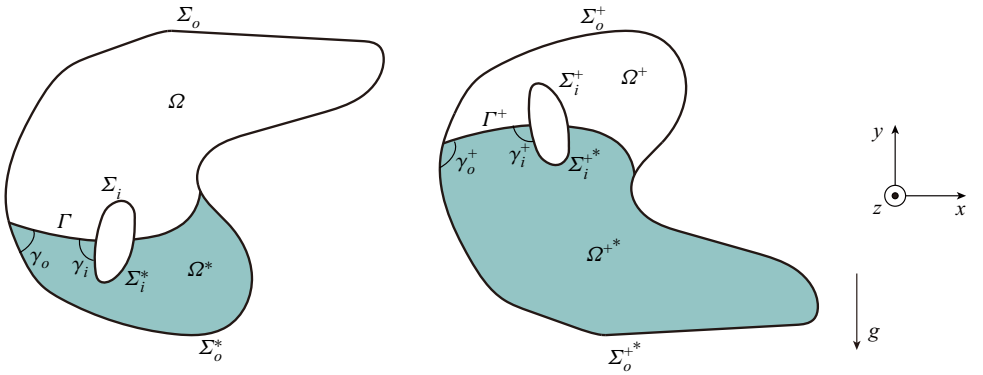

Figure 11. Schematic of cross-section of a horizontal tube Ω in an arbitrary geometrical shape and the cross-section of another horizontal tube Ω^+ whose perimeter is symmetric to the perimeter of the cross-section Ω with respect to the horizontal axis.

It is concluded that the critical Bond number(s) for the vertical upward eccentricity at a contact angle is equal to the case of the vertical downward eccentricity having equal magnitude of the vertical upward eccentricity at the supplementary contact angle, which can also be demonstrated by the curves in the first and third graphs of figure 3 of Rascón *et al*. (2016).

Furthermore, for the horizontal eccentricity, the perimeter of the tube cross-section is symmetric with respect to the horizontal line of symmetry of the cross-section. Therefore, the critical emptying line is symmetric about the vertical line $\gamma_o = \gamma_i = \gamma = 90°$, which is demonstrated by the tubes each of which has one cross-section in another shape being symmetric with respect to the horizontal line of symmetry of the cross-section (Manning *et al.* 2011; Manning & Collicott 2015; Rascón *et al.* 2016; Zhu *et al.* 2020; Zhou *et al.* 2021).

Under zero gravity, the shape of a liquid droplet in an eccentric annular tube is independent of the eccentric angle. In this case, the energy Φ for contact angles γ_i and γ_o and an interface Γ for an eccentric annular tube is equal to the energy Φ^+ for $\gamma_i^+ = 180°-\gamma_i$ and $\gamma_o^+ = 180°-\gamma_o$, and $|\Gamma^+| = |\Gamma|$ for the tube. If $\Phi_{min} = 0$ at contact angles γ_i and γ_o, then $\Phi_{min}^+ = 0$ will exist at contact angles $180° - \gamma_i$ and $180° - \gamma_o$, for the tube. The contact angle corresponding to point J (figure 2*b*) is the supplementary contact angle corresponding to point K (figure 2*b*).

Appendix B

At zero Bond number, the energy functional (2.8) becomes

$$\Phi = |\Gamma| - (|\Sigma_o^*| \cos\gamma_o + |\Sigma_i^*| \cos\gamma_i) + \lambda|\Omega^*|, \tag{B1}$$

where the Lagrange parameter λ is obtained from (2.5) as $\lambda = 2(\cos\gamma_o + \chi\cos\gamma_i)/[R_o(1-\chi^2)]$, and the 2-D gas–liquid interface becomes a circular arc, the radius of which is given by

$$R_s = \frac{1}{\lambda} = \frac{R_o(1-\chi^2)}{2(\cos\ \gamma_o + \chi\cos\gamma_i)}. \tag{B2}$$

The interface is convex towards the liquid for $R_s > 0$ and concave towards the liquid for $R_s < 0$. The following analyses are suitable for $R_s > 0$ and $R_s < 0$. As gravity vanishes, the

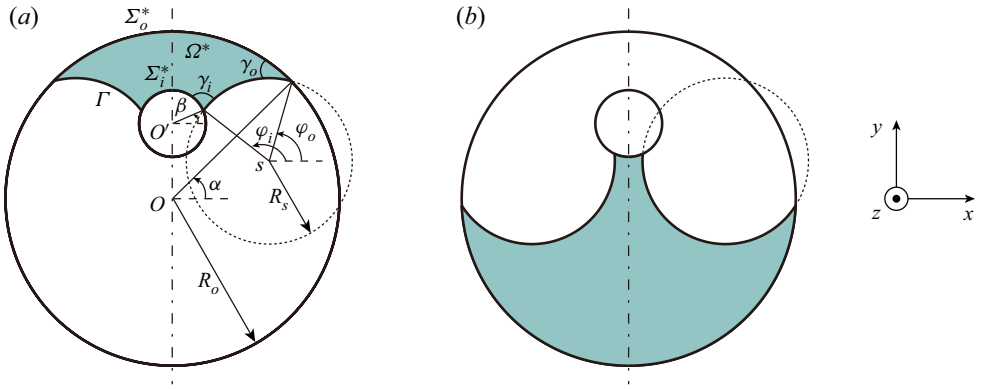

Figure 12. Non-occluded liquid configurations with the interface meeting the outer and inner walls at zero gravity for a set of inner and outer contact angles γ_i and γ_o. The liquid may occupy (*a*) the narrow part or (*b*) the wide part. In (*a*), α is the angular position of the outer contact point on the outer circle, β is the angular position of the inner contact point on the inner circle and φ_o and φ_i are the angular positions of the outer and inner contact points on the interface arc, respectively. These angular positions are measured counterclockwise, starting from the positive x axis.

configuration of liquid in an eccentric annular cross-section is independent of the eccentric angle θ and symmetric with respect to the axis of symmetry (through the line OO') of the cross-section.

The non-occluded liquid configurations for the cases under zero gravity can be divided into three types: the interface only meeting the outer wall, the interface only meeting the inner wall and the interface meeting the outer and inner walls. We found that the values of energy functional Φ for the former two types are always larger than 0. The two types will not be considered here for calculation of the critical parameters corresponding to zero Bo_c.

For the non-occluded liquid configuration with the interface meeting the outer and inner walls for a set of geometric parameters R_o, χ and e, and the contact angles γ_i and γ_o, the liquid may occupy the narrow part (figure 12*a*) or the wide part (figure 12*b*), and the location of the interface as shown in figure 12(*a*,*b*) can be determined by the geometrical relationship due to zero Bond number. The centre s of curvature of the interface segment on the right-hand side of the cross-section for each of the two cases as shown in figure 12(*a*,*b*) has coordinates (x_s, y_s), where x_s and y_s are given by, respectively,

$$x_s = \sqrt{R_s^2 + R_o^2 - 2R_sR_o\cos\gamma_o}\,\sin\left[\cos^{-1}\left(\frac{eR_o}{2\sqrt{R_s^2 + R_o^2 - 2R_sR_o\,\cos\,\gamma_o}}\right)\right], \quad \text{(B3}a\text{)}$$

$$y_s = \frac{eR_o}{2}. \quad \text{(B3}b\text{)}$$

By considering the case that the liquid is wrapped in the narrow part (figure 12*a*), the angular position of the outer contact point on the outer circle, α, the angular position of the inner contact point on the inner circle, β, and the angular positions of the outer and inner contact points on the interface arc, φ_o and φ_i, are given by, respectively,

$$\alpha = \mathrm{sgn}(R_s)\cos^{-1}\left(\frac{R_o - R_s\cos\gamma_o}{\sqrt{R_s^2 + R_o^2 - 2R_sR_o\cos\gamma_o}}\right) + \tan^{-1}\left(\frac{y_s}{x_s}\right), \quad \text{(B4}a\text{)}$$

$$\beta = \mathrm{sgn}(R_s)\cos^{-1}\left(\frac{\chi R_o + R_s\cos\gamma_i}{\sqrt{R_s^2 + (\chi R_o)^2 + 2\chi R_o R_s\cos\gamma_i}}\right) - \tan^{-1}\left(\frac{y_s}{x_s}\right), \tag{B4b}$$

$$\varphi_o = \alpha + \gamma_o, \quad \varphi_i = \beta + \pi - \gamma_i. \tag{B4c,d}$$

Due to the symmetry of the cross-section, the lengths of the liquid boundary parameters Γ, Σ_o^* and Σ_i^* can be expressed as

$$|\Gamma| = 2R_s(\varphi_i - \varphi_o), \quad |\Sigma_o^*| = R_o(\pi - 2\alpha), \quad |\Sigma_i^*| = \chi R_o(\pi - 2\beta). \tag{B5a–c}$$

By the application of the Green formula, the liquid area becomes (Pour & Thiessen 2019)

$$|\Omega^*| = R_o^2\left(\frac{\pi}{2} - \alpha\right) + \chi R_o^2\left(\chi\beta - e\cos\beta - \frac{\pi\chi}{2}\right) + R_s^2(\varphi_o - \varphi_i) + R_s[x_s(\sin\varphi_o - \sin\varphi_i) - y_s(\cos\varphi_o - \cos\varphi_i)]. \tag{B5d}$$

Then, the value of energy functional for the case of liquid occupying the narrow part Φ_n can be calculated from (B1).

For the case of liquid wrapped in the wide part (figure 12*b*), the above equations (B4) and (B5) are not suitable due to the geometrical relationship. According to Appendix A, the energy functional for the case of liquid occupying the wide part Φ_w for a set of contact angles γ_i and γ_o will be equal to Φ_n for another set of contact angles $180^\circ - \gamma_i$ and $180^\circ - \gamma_o$, which can be calculated using the above equations. Parameter Φ_{min} is determined, which is equal to the minimum value of Φ_n and Φ_w. One can repeat the above steps by changing the geometric parameters R_o, χ and e, and the contact angles γ_i and γ_o to find the critical parameters of geometry and contact angles corresponding to zero critical Bond number that lets $\Phi_{min} = 0$.

References

Bhatnagar, R. & Finn, R. 2016 On the capillarity equation in two dimensions. *J. Math. Fluid Mech.* **18**, 731–738.

Brakke, K.A. 1992 The surface evolver. *Exp. Maths* **1**, 141–165.

Carrasco-Teja, M., Frigaard, I.A., Seymour, B.R. & Storey, S. 2008 Viscoplastic fluid displacements in horizontal narrow eccentric annuli: stratification and travelling wave solutions. *J. Fluid Mech.* **605**, 293–327.

Chen, Y. & Collicott, S.H. 2006 Study of wetting in an asymmetrical vane-wall gap in propellant tanks. *AIAA J.* **44**, 859–867.

Choueiri, G.H. & Tavoularis, S. 2015 Experimental investigation of flow development and gap vortex street in an eccentric annular channel. Part 2. Effects of inlet conditions, diameter ratio, eccentricity and Reynolds number. *J. Fluid Mech.* **768**, 294–315.

Concus, P. & Finn, R. 1969 On the behavior of a capillary surface in a wedge. *Proc. Natl Acad. Sci. USA* **63**, 292–299.

Finn, R. 1986 *Equilibrium Capillary Surfaces*. Springer-Verlag.

Lamarche-Gagnon, M-É & Tavoularis, S. 2021 Further experiments and analysis on flow instability in eccentric annular channels. *J. Fluid Mech.* **915**, A34.

Lee, C.C., Wu, A. & Li, M. 2020 Venous air embolism during neurosurgery. In *Essentials of Neurosurgical Anesthesia & Critical Care: Strategies for Prevention, Early Detection, and Successful Management of Perioperative Complications*, pp. 287–291. Springer International Publishing.

Manning, R., Collicott, S. & Finn, R. 2011 Occlusion criteria in tubes under transverse body forces. *J. Fluid Mech.* **682**, 397–414.

Manning, R.E. & Collicott, S.H. 2015 Existence of static capillary plugs in horizontal rectangular cylinders. *Microfluid Nanofluid* **19**, 1159–1168.

Nikitin, N., Wang, H. & Chernyshenko, S. 2009 Turbulent flow and heat transfer in eccentric annulus. *J. Fluid Mech.* **638**, 95–116.

PARRY, A.O., RASCÓN, C., JAMIE, E.A.G. & AARTS, D.G.A.L. 2012 Capillary emptying and shortrange wetting. *Phys. Rev. Lett.* **108** (24), 246101.

POUR, N.B. & THIESSEN, D.B. 2019 Equilibrium configurations of drops or bubbles in an eccentric annulus. *J. Fluid Mech.* **863**, 364–385.

PROTIERE, S., DUPRAT, C. & STONE, H.A. 2013 Wetting on two parallel fibers: drop to column transitions. *Soft Matt.* **9** (1), 271–276.

RASCÓN, C., PARRY, A.O. & AARTS, D.G.A.L. 2016 Geometry-induced capillary emptying. *Proc. Natl Acad. Sci. USA* **113**, 12633–12636.

RENTERIA, A. & FRIGAARD, I.A. 2020 Primary cementing of horizontal wells. Displacement flows in eccentric horizontal annuli. Part 1. Experiments. *J. Fluid Mech.* **905**, A7.

REYSSAT, E. 2015 Capillary bridges between a plane and a cylindrical wall. *J. Fluid Mech.* **773**, R1.

SMEDLEY, G. 1990 Containments for liquids at zero gravity. *Microgravity Sci. Technol.* **3**, 13–23.

VERMA, G., SARAJ, C.S., YADAV, G., SINGH, S.C. & GUO, C. 2020 Generalized emptying criteria for finite-lengthed capillary. *Phys. Rev. Fluids* **5**, 112201(R).

ZHANG, F.Y., YANG, X.G. & WANG, C.Y. 2006 Liquid water removal from a polymer electrolyte fuel cell. *J. Electrochem. Soc.* **153**, A225–A232.

ZHOU, X. & ZHANG, F. 2017 Bifurcation of a partially immersed plate between two parallel plates. *J. Fluid Mech.* **817**, 122–137.

ZHOU, X., ZHANG, G., ZHU, C., TAN, D. & FU, C. 2021 Inside rod induced horizontal capillary emptying. *J. Fluid Mech.* **924**, A23.

ZHU, C., ZHOU, X. & ZHANG, G. 2020 Capillary plugs in horizontal rectangular tubes with non-uniform contact angles. *J. Fluid Mech.* **901**, R1.